

Modeling study of synergistic effects of neutral beam injection hot ions on helicon wave current drive in HL-3 tokamak

Shu-Heng Sun(孙书恒), Dao-Zheng Zi(资道政), Zu-Guang Liu(刘祖光), Sen Wang(王森), and Xin-Xia Li(李新霞)
Citation: Chin. Phys. B, 2026, 35 (**3**): 035203. DOI: 10.1088/1674-1056/adf17e
http://cpb.iphy.ac.cn; http://iopscience.iop.org/cpb

What follows is a list of articles you may be interested in

Quantified causality dependence of dynamical relation between zonal flow and heat transport on isotope mass in tokamak edge plasmas

Yu He(何钰), Zhongbing Shi(石中兵), Yuhong Xu(许宇鸿), Jun Cheng(程钧), Jianqiang Xu(许健强), Zhihui Huang(黄治辉), Na Wu(吴娜), Kaiyang Yi(弋开阳), Weice Wang(王威策), Min Jiang(蒋敏), Longwen Yan(严龙文), Xiaoquan Ji(季小全), and Wulyu Zhong(钟武律)
Chin. Phys. B, 2025, 34 (**10**): 105202. DOI: 10.1088/1674-1056/ade069

Effects of diamagnetic drift on nonlinear interaction between multi-helicity neoclassical tearing modes

Haiyuan Wang(王海源), Shuai Jiang(姜帅), Tong Liu(刘桐), Lai Wei(魏来), Qibin Luan(栾其斌), and Zheng-Xiong Wang(王正汹)
Chin. Phys. B, 2024, 33 (**6**): 065202. DOI: 10.1088/1674-1056/ad24d3

Simulation of deuterium pellet ablation and deposition in the EAST tokamak with HPI2 code

Da-Zheng Li(李大正), Jie Zhang(张洁), Ji-Lei Hou(侯吉磊), Mao Li(李懋), and Ji-Zhong Sun(孙继忠)
Chin. Phys. B, 2024, 33 (**4**): 045204. DOI: 10.1088/1674-1056/ad1e68

Wave field structure and power coupling features of blue-core helicon plasma driven by various antenna geometries and frequencies

Chao Wang(王超), Jia Liu(刘佳), Lei Chang(苌磊), Ling-Feng Lu(卢凌峰), Shi-Jie Zhang(张世杰), and Fan-Tao Zhou(周帆涛)
Chin. Phys. B, 2024, 33 (**3**): 035201. DOI: 10.1088/1674-1056/ad1486

Synthesis of SiC/graphene nanosheet composites by helicon wave plasma

Jia-Li Chen(陈佳丽), Pei-Yu Ji(季佩宇), Cheng-Gang Jin(金成刚), Lan-Jian Zhuge(诸葛兰剑), and Xue-Mei Wu(吴雪梅)
Chin. Phys. B, 2021, 30 (**7**): 075201. DOI: 10.1088/1674-1056/abe1a1

Modeling study of synergistic effects of neutral beam injection hot ions on helicon wave current drive in HL-3 tokamak

Shu-Heng Sun(孙书恒)[1], Dao-Zheng Zi(资道政)[1], Zu-Guang Liu(刘祖光)[1], Sen Wang(王森)[1], and Xin-Xia Li(李新霞)[1,2,†]

[1] *School of Nuclear Science and Technology, University of South China, Hengyang* 421001, *China*
[2] *Key Laboratory of Advanced Nuclear Energy Design and Safety, Ministry of Education, Hengyang* 421001, *China*

(Received 9 May 2025; revised manuscript received 30 June 2025; accepted manuscript online 18 July 2025)

Helicon waves with very high ion cyclotron harmonics have been proposed for active off-axis current drive in tokamak with high performance operations. Under the application of ion cyclotron resonant heating or the neutral beam injection, hot ions with very high energy exist. For helicon waves with a wave frequency of 476 MHz and $n_{\parallel} = 3.0$, as utilized in DIII-D and KSTAR tokamaks, theoretical analysis based on the fast wave dispersion relation indicates that the ion damping coefficient can be comparable to electron damping coefficient once the hot ions are injected. The synergistic effects of hot ions produced by neutral beam injection on helicon wave current drive in the HL-3 tokamak are investigated numerically using GENRAY/CQL3D simulations. The results indicate that electron damping remains the dominant mechanism owing to the low concentration of hot ions, and robust off-axis current drive can generally be achieved in the device. Considering the hot ions with an average energy $\langle E_{\rm avg}\rangle \sim 80$ keV produced by neutral beam injection, positive synergistic effects between the hot ions and the helicon wave are observed, where super hot ions with energy exceeding 100 keV appear, as evidenced by the formation of a pronounced plateau in the hot ion velocity distribution function. Finally, the introduction of minority hot ions is proved to have a limited effect on the total current drive in the device.

Keywords: hot ions, helicon wave, tokamak, HL-3

PACS: 52.55.Fa, 52.55.Wq

DOI: 10.1088/1674-1056/adf17e **CSTR:** 32038.14.CPB.adf17e

1. Introduction

Helicon wave, *i.e.*, the fast magnetosonic wave at fairly high ion cyclotron harmonics, has been proposed for active off-axis current drive in advanced tokamaks with high plasma beta, especially for the tokamak reactors, such as ITER, FNAS-AT, CFETR, and so on.[1–4] Analysis of the fast wave dispersion relation indicates that high wave frequency makes the waves exhibit whistler-like behavior, but with a small perpendicular (radial) component that allows the wave rays to penetrate into the core plasma.[5] Consequently, the wave rays can propagate long distances through off-axis regions, providing high current drive efficiency. Modeling calculations on the FNAS-AT and DIII-D tokamak in high performance discharges indicate that robust off-axis current drive with good efficiency can be generally achieved once electron beta $\beta_{\rm e}$ exceeds 1.8%.[1,2] For DIII-D discharge 122797, GENRAY simulations predict that a 500-MHz helicon wave can drive up to 60 kA/MW, with an efficiency 2 to 4 times higher than that of neutral beam current drive or electron cyclotron current drive. Using the same wave parameters, full wave calculations based on the AORSA code, with the scrape-off layer (SOL) neglected, reproduce both the profile and magnitude of the driven current predicted by GENRAY code for the envisioned high β scenarios in DIII-D.[1,6] For the CFETR device, the off-axis current drive is proven to be insensitive to the launched value of the parallel index of refraction $n_{\parallel}$ when wave frequency is greater than 1 GHz.[3] In addition, modeling calculations on HL-3 and EAST tokamaks have recently demonstrated a positive synergistic effect of current drive when helicon waves are combined with lower hybrid wave injection.[7–9]

In addition to significant achievements in theoretical analysis, substantial progress has also been made in the engineering deployment of helicon waves. In KSTAR device, the helicon wave system is currently being upgraded with 1.2-MW klystrons at wave frequency 476 MHz,[10] and the new antenna design is capable of handling MW-class RF power in terms of peak electric field.[11] A 1-MW high power helicon system has been conducted in DIII-D device, where a 30-module comb-line traveling wave array antenna (TWA) with wave frequency of 476 MHz has been installed and optimized in-vessel, and the preliminary measurements show that both the reflected power and dissipated power of each module can be maintained below 2%.[12] Moreover, significant electron heating in the core plasma has been observed during the helicon wave launching.[13]

Among these works, the wave absorption is calculated

†Corresponding author. E-mail: li_xx@usc.edu.cn

© 2026 Chinese Physical Society and IOP Publishing Ltd. All rights, including for text and data mining, AI training, and similar technologies, are reserved.

by electron Landau damping combined with transit-time magnetic pumping (TTMP), where a single pass absorption of the wave power is dominant. This treatment is usually feasible since the ions' wave damping is very weak under high ion cyclotron frequency.[4,7] However, the fast wave dispersive relation indicates that ion damping can increase dramatically at high ions temperature,[14] especially for the fast ions that conducted by the ion cyclotron resonant heating (ICRH) process or neutral beam injection (NBI). Specifically, as the hydrogen (H) ions are present, this phenomenon becomes more pronounced due to their higher velocity and lower harmonic number compared to deuterium (D) ions.[14] It is therefore crucial to quantify the impact of hot ions on helicon wave current drive in tokamak plasmas for its further application.

In this paper, we perform a model calculation of H and D hot ions in the performance of helicon wave current drive in HL-3 tokamak under wave frequency 476 MHz. The synergistic effects of hot ions' energy together with their concentration are also investigated using GENRAY/CQL3D simulations.

2. Physical model and wave absorption

In a warm Maxwellian plasma, the helicon wave absorption of electrons is approximated by[15]

$$k_{\perp \mathrm{I}}^{(\mathrm{e})} = \frac{\sqrt{\pi}}{4} k_{\perp} \beta_{\mathrm{e}} \xi_{\mathrm{e}} \, \mathrm{e}^{-\xi_{\mathrm{e}}^2} G, \tag{1}$$

where $\xi_{\mathrm{e}} = \upsilon_{\parallel}/\upsilon_{\mathrm{te}} = c/n_{\parallel}\upsilon_{\mathrm{te}}$, $\upsilon_{\parallel}$ is the phase velocity of the wave parallel to the magnetic field, $\upsilon_{\mathrm{te}} = \sqrt{2\kappa T_{\mathrm{e}}/m_{\mathrm{e}}}$ is the electron thermal speed, $n_{\parallel}$ is the parallel refractive index, and c denotes the speed of light, $\beta_{\mathrm{e}} \equiv 8\pi n_{\mathrm{e}} \kappa T_{\mathrm{e}}/B^2$ is defined as the electron beta and κ is the Boltzmann constant. $k_{\perp}$ is the perpendicular wave number, given by

$$k_{\perp} = \frac{\omega}{c} \sqrt{\frac{(S-n_{\parallel}^2)^2 - D^2}{S - n_{\parallel}^2 + D^2 \frac{\mathrm{Re}(\varepsilon_{33})}{|\varepsilon_{33}|^2} \frac{n_{\parallel}^2}{S-n_{\parallel}^2}}}, \tag{2}$$

where S and D are cold plasma Stix parameters, $\varepsilon_{33} = X\omega_{\mathrm{pe}}/\omega$ is an element of the dielectric matrix and ω_{pe} is the electron plasma frequency, $X = 2\xi_{\mathrm{e}}^2[1 + \xi_{\mathrm{e}} Z(\xi_{\mathrm{e}})]$, and $Z(\xi_{\mathrm{e}})$ is the plasma dispersion function.[16] G is referred to wave damping factor.[15]

As the wave passes cross ion cyclotron harmonic resonances, ion damping occurs and can be obtained in a way analogous to electron damping,[15] where

$$k_{\perp \mathrm{I}}^{(\mathrm{i})} = \frac{k_{\perp R}}{2} \left[\frac{\varepsilon_{11}^{(\mathrm{I})} - \frac{2D\varepsilon_{33}^{(\mathrm{R})}}{|\varepsilon_{33}|^2} \varepsilon_{12}^{(\mathrm{R})}}{A_2} + \frac{(S-n_{\parallel}^2)(\varepsilon_{22}^{(\mathrm{I})} + \varepsilon_{11}^{(\mathrm{I})}) - 2D\varepsilon_{12}^{(\mathrm{R})}}{(S-n_{\parallel}^2)^2 - D^2} \frac{A_1}{A_2} \right]. \tag{3}$$

Among these equations, the superscript and subscript symbols e, i, R, and I represent species of electrons and ions, real parts, and imaginary parts, respectively. A_1 and A_2 can be found in Ref. [15]. Once the hot ions are taken into account, the calculation of each element in the dielectric matrix is obtained by summing over all ions species.

The wave power deposition can be calculated along the wave rays trajectory, where

$$P(l) = P(0) \exp\left(-2 \int_0^l k_{\perp \mathrm{I}}^{(\alpha)} \, \mathrm{d}l \right). \tag{4}$$

Here, $P(0)$ is the initial incident power, and the symbol α denotes the electron and each species ions, respectively. Simultaneously, the current drive is given by $j = \eta P$, with η denoting the current drive efficiency. In the paper, the wave trajectory is calculated by the GENRAY ray tracing code, and the current drive efficiency can be evaluated by Ehst–Karney formula.[17]

On the other hand, by putting the wave information into the CQL3D quasilinear current drive code, the current drive can be calculated by[18]

$$J(r) = n_{\alpha} q(r) \int v_{\parallel} f(v) \, \mathrm{d}v_{\parallel}. \tag{5}$$

This expression gives the parallel current density carried by each species, where n_{α} is the density of the particle α and $q(r)$ is the associated charge. In the equation above, $v_{\parallel}$ is the speed component that is parallel to the magnetic field lines, $f(v)$ is the phase-space distribution of species, which obeys[17]

$$\frac{\partial f_{\alpha}}{\partial t} = \frac{\partial}{\partial v_{\parallel}} D_{\mathrm{ql}} \frac{\partial f_{\alpha}}{\partial v_{\parallel}} + C(f_{\alpha}) - \frac{1}{r} \frac{\partial}{\partial r} \left(r D_{\mathrm{st}} \frac{\partial f_{\alpha}}{\partial r} \right). \tag{6}$$

Here, $D_{\mathrm{ql}} = \pi \frac{q^2}{m^2} E_{1k}^2 \delta(\omega - k v_{\parallel}) \, \mathrm{d}k$ is the quasi-linear diffusion coefficient in velocity space, r is the normalized minor radius. On the right-hand side of Eq. (6), the first term represents the contribution from radio frequency waves, the second term is the Coulomb collision operator of the plasma species and D_{st} denotes its radial diffusion coefficient. In the presence of hot ions, a significant portion of wave power can be deposited onto these ions, leading to the generation of super hot ions. Consequently, both the electrons and hot ions evolve according to Eq. (6), while active energy exchange occurs owing to Coulomb collisions.

3. Results and discussion

Using the FW dispersion relation,[15] the influence of hot ions on wave absorption mechanism can be quantified through the wave damping coefficient. Figure 1 plots the wave damping coefficient $k_{\perp \mathrm{I}}$ as a function of the parallel refractive index $n_{\parallel}$ for a launch frequency of 476 MHz. The plasma parameters are taken at the radial position $\rho = 0.5$ according

to the stable state operation scenario in HL-3,[8,19–21] where $n_e = 3.47 \times 10^{19}$ m^{-3}, $T_e = 5.44$ keV, and $T_i = 6.96$ keV. The hot ions hydrogen with averaged energy $E_{avg} = 80$ keV and concentration $X[\mathrm{H}] = n_H/n_e = 5\%$ are illustrated in the figure.[22] It is clearly shown that electron damping increases monotonically, peaking at $n_{\|} \sim 3.8$. In contrast, damping on bulk ions remains negligible (green dashed curve), confirming earlier predictions that ion power deposition can be neglected for helicon current drive.[1,7,23] However, with the presence of hot ions, enormous wave damping on ions occurs, especially for minority ions hydrogen. For $n_{\|} \sim 3.0$, the ion damping coefficient is shown to be comparable to that on electrons.

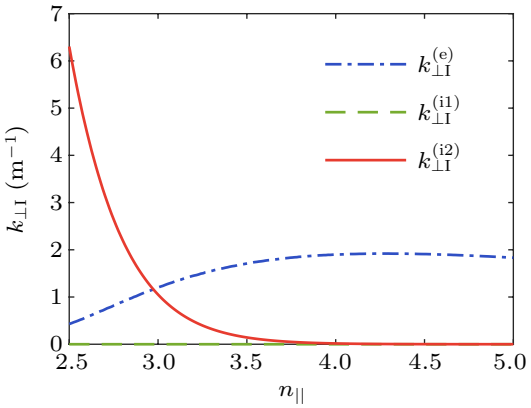


Fig. 1. The wave damping coefficients $k_{\perp \mathrm{I}}$ on ions and electrons as a function of the parallel refractive index $n_{\|}$. The wave damping coefficients of electron and ions are denoted by $k_{\perp \mathrm{I}}^{(\mathrm{e})}$ and $k_{\perp \mathrm{I}}^{(\mathrm{i})}$, respectively. $k_{\perp \mathrm{I}}^{(\mathrm{i1})}$ and $k_{\perp \mathrm{I}}^{(\mathrm{i2})}$ are the ion damping coefficient of $X[\mathrm{D}] = 100\%$ and $X[\mathrm{D}] = 95\%$ with $X[\mathrm{H}] = 5\%$, respectively. The plasma parameters are taken at $\rho = 0.5$ of the stable state operation scenario on HL-3, where $n_e = 3.47 \times 10^{19}$ m^{-3}, $T_e = 5.44$ keV, $T_i = 6.96$ keV, and $B = 2.0$ T. The energy of hot ions is set as $E_{avg} = 80$ keV.

Figure 2 depicts the poloidal trajectories of helicon wave rays. The equilibrium is derived from an integrated METIS simulation of the HL-3 steady-state scenario of S3 with deuterium plasma.[24,25] This code has been benchmarked against previous HL-2A discharges. The major radius and minor radius are $R = 1.78$ m and $a = 0.65$ m, respectively. For a launch frequency of 476 MHz and $n_{\|} \sim 3.0$, it is straightforward to get $\lambda_{\perp} < 2.0$ cm $\ll a$, warranting the use of the GENRAY ray-tracing code. The wave rays are emitted from three poloidal launch points, each comprising 20 rays to represent the antenna power spectrum. The power injected is set at 1 MW with $n_{\|} \sim 3.0 \pm 0.5$, while 10% of the power is launched in the counter direction with $n_{\|} \sim -9.0$, consistent with measurements on the KSTAR helicon antenna.[11] Rays originate just inside the last closed flux surface ($\rho = 0.99$) and are tracked until 99% of the power has been absorbed. The calculations show that the rays penetrate directly into the core plasma, and single-pass absorption appears. However, when minority hot ions are considered, only a very slight change in the ray trajectories is observed.

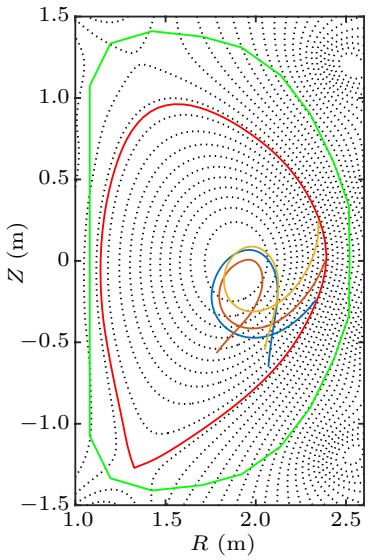


Fig. 2. Poloidal projection of the helicon wave rays trajectory in HL-3. The wave rays are launched from 3 points along the poloidal direction, each ray starting at the mid-plane inside the last closed flux surface $\rho = 0.99$. The helicon wave parameters are set as $f = 476$ MHz and $n_{\|} = 3.0$. The red thick line represents the last closed flux surface.

However, significant power deposition on ions is found as hot ions are present, as plotted in Fig. 3. In the figure, minority hot ions hydrogen with $\langle E \rangle = 80$ keV are taken into account. For $X[\mathrm{H}] = 10\%$, about 8% of the injected power is absorbed by ions. The fraction rises further as the hot ion energy increases. Replacing the hydrogen minority with deuterium markedly reduces ion absorption, which is in good agreement with Ono's prediction.[14]

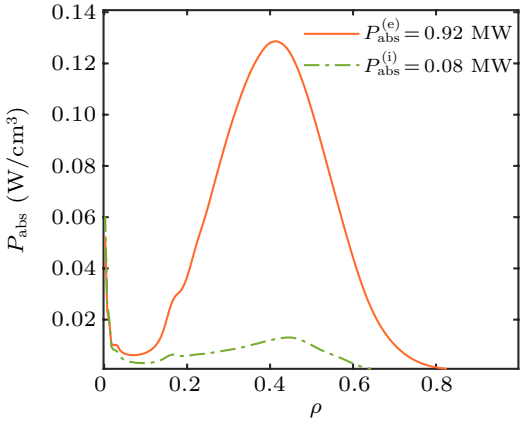


Fig. 3. Power absorption profile calculated by GENRAY code. The solid line indicates power absorbed by electrons, while the dashed line represents absorption by ions. The total power injected $P = 1$ MW. The hot ion H concentration $X[\mathrm{H}] = 10\%$.

The helicon wave current drive with the presence of hot ions is plotted in Fig. 4. Here, the calculation is performed by the CQL3D method, where both the electrons and hot ions are treated as general particles and evolve according to Eq. (6). The radial current drive profile is essentially unchanged. However, the share of power absorption by the ions slightly reduces electron absorption and thus produces a small drop in the net driven current.

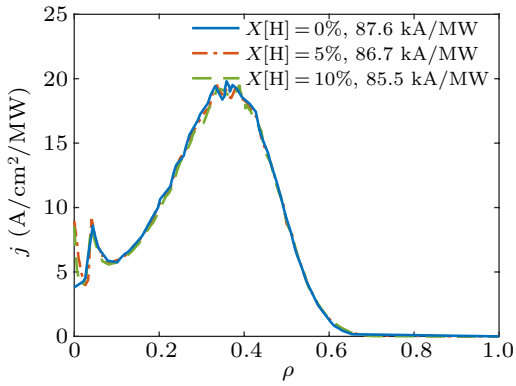


Fig. 4. The current drive profiles calculated by the CQL3D code under various hot ion H concentrations X[H]. Both the electrons and the hot ions evolve according to Eq. (6). The average energy of hot ions hydrogen is $\langle E\rangle = 80$ keV.

Table 1 gives the current drive for various hot ions concentrations, only a few percent of the current drive occurs on ions. However, it is worth mentioning that this phenomenon may become serious if higher energy hot ions exists.

Table 1. Scans of hot ion hydrogen concentrations X[H] on the current drive that pushed by electron and ion. The calculations are performed by the CQL3D code.

X[H]	I_e (kA)	I_i (A)
0.00	87.6	3.1
0.02	87.4	12.1
0.04	86.9	24.2
0.06	86.5	36.3
0.08	86.0	48.2
0.10	85.6	60.2

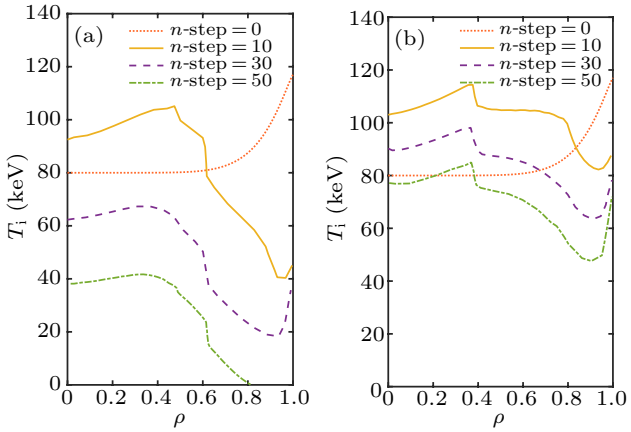


Fig. 5. Evolution of radial temperature profiles of different hot particles at various time steps. Panel (a) shows hot hydrogen (H) and panel (b) shows hot deuterium (D). The time steps are 0, 10, 20, and 40, with a time interval of 0.01 s.

In the presence of hot ions, a significant portion of the wave power is absorbed by the ions. We therefore employed the CQL3D code to track their temporal evolution, as shown in Fig. 5. Figures 5(a) and 5(b) correspond to minority hydrogen and deuterium, respectively. The hot ions are assumed to originate from NBI with an initial average energy of $E_{avg} = 80$ keV, their radial energy distribution at $t = 0$ s is indicated by the orange dotted curve. Here, these hot ions are treated as the additional ions in the simulations. Energy spectra at 10, 30, and 50 time steps are also plotted. It is clearly shown that super-hot ions with energy up to $E \sim 100$ keV are produced, followed by a gradual decay of their energies owing to Coulomb collisions. Since hydrogen has a smaller mass, the energy of its super-hot ions decreases more rapidly than that of deuterium, and by the 40th time step, it has fallen below the initial energy profile. Moreover, energy in the plasma edge decays most rapidly, consistent with the lower temperature and higher collision frequency in that region.

In addition, figure 6 presents the velocity distribution function of the fast ions. Wave energy deposition produces a pronounced plateau, visible in all representative pitch angle traces, and thus confirms the formation of super-hot ions.

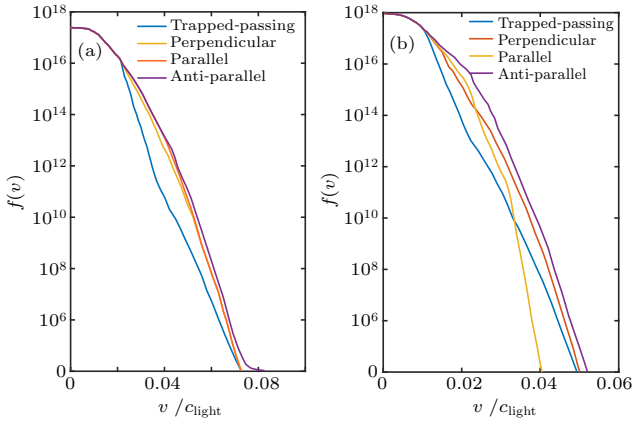


Fig. 6. Illustration of hot ion distribution function, shown at the midplane for $\rho = 0.58$ ($R = 103$ cm) and $t = 0.5$ s. Panel (a) shows hot hydrogen (H) and panel (b) shows hot deuterium (D). $c_{light} = 3 \times 10^8$ m/s. Four sets of curves are plotted, corresponding to the selected values of pitch angles (at parallel, trapped-passing, perpendicular, and anti-parallel).

4. Summary and discussion

The HL-3 device is a newly constructed medium-sized tokamak in China. Equipped with an NBI system, HL-3 has achieved a 'dual-billion-degree' regime with both ion and electron temperatures reach the 10 keV range. Its engineering parameters are closely comparable to those of the DIII-D tokamak. In recent years, DIII-D and KSTAR devices have conducted pioneering experiments on helicon wave current drive, leading to significant advancements in plasma discharge sustainability. Consequently, investigating helicon wave related physical mechanisms on HL-3 could provide novel approaches to enhance high-performance operation on the device.

In this work, we include the hot ions as general species. The evolution of the hot ions distribution is obtained using the bounce-averaged quasilinear Fokker–Planck equation. Under the steady-state scenario on HL-3, our calculations show that minority hydrogen or deuterium ions with energies around 80 keV possess wave damping coefficients comparable to those of electrons, so a non-negligible fraction of the injected power is absorbed by the ions. This additional absorption has

little effect on the radial profile of the driven current, yet it accelerates a subset of the minority ions to super-hot energies of $\sim$ 100 keV. In the core plasma, these super-hot deuterons persist longer than the hydrogen counterparts due to their larger mass and lower collisional energy loss. Compared with the case in ICRF, the energy of these super hot ions is significantly lower. This is due to the rapid decrease in the ion damping coefficient with increasing harmonic number of the wave frequency. Consequently, in the helicon wave process, the conversion of hot ions into super hot ions is markedly weaker than in the ICRF case.

Fast wave dispersion analysis further indicates that elevating the minority ion temperature, whether by increasing NBI energy or generating higher energy ions via ICRH, enhances the contribution of hot ions, particularly for high-energy α particles produced in fusion reactions. Under such conditions, the ion damping coefficient can exceed that of electron damping, introducing additional physical phenomena associated with the large gyro-radius of these ions. A rigorous theoretical framework must therefore incorporate finite-orbit-width (FOW) effects, for instance, the FOW-CQL3D methodology will be systematically investigated in our subsequent work.

Data availability statement

The data that support the findings of this study are openly available in the Science Data Bank at the following link https://doi.org/10.57760/sciencedb.j00113.00274.

Acknowledgements

Project supported by the Natural Science Foundation of Hunan Province, China (Grant No. 2026JJ50354) and Hunan Province College Students' Innovative Experimental (Grant Nos. S202410555204 and S202410555199).

References

[1] Prater R, Moeller C P, Pinsker R I, Porkolab M, Meneghini O and Vdovin V 2014 *Nucl. Fusion* **54** 083024
[2] Prater R, Pinsker R, Moeller C, Porkolab M and Vdovin V 2014 *AIP Conference Proceedings* Vol. 1580 (American Institute of Physics) pp. 247–250
[3] Yang Y Q, Zhang X J, Zhao Y P, Qin C M, Mao Y Z and Yang H 2020 *AIP Conference Proceedings* **2254** 060004
[4] Li X, Li G and Liu H 2021 *Fusion Engineering and Design* **172** 112897
[5] Vdovin V 2013 *Plasma Physics Reports* **39** 95
[6] Lau C, Jaeger E, Bertelli N, Berry L A, Green D L, Murakami M, Park J M, Pinsker R I and Prater R 2018 *Nucl. Fusion* **58** 066004
[7] Zi D Z, Cheng Z H, Sun S H, Li M H and Li X X 2025 *Fusion Engineering and Design* **215** 114968
[8] Liu G N, Li X X, Liu H B and Sun A P 2023 *Acta Phys. Sin.* **72** 245202 (in Chinese)
[9] Yin L, Zheng P, Gong X, Yang C, Yin X, Song C, Huang Q, Chen Y and Zhong Y 2022 *Nuclear Fusion* **62** 066023
[10] Kim J, Wang S, Jang K, Lee H and Wi H 2021 *Fusion Engineering and Design* **166** 112301
[11] Wi H, Wang S, Kim J and Kwak J 2023 *Fusion Engineering and Design* **195** 113983
[12] Compernolle B V, Brookman M W, Moeller C P, Pinsker R I, Garofalo A M, O'Neill R, Geng D, Nagy A, Squire J P and Schultz K 2021 *Nucl. Fusion* **61** 116034
[13] Pinsker R, Van Compernolle B, Tang S, Lestz J, Moeller C, Petty C, Dupuy A, Squire J, Garofalo A, Porkolab M, Rost J, Baek S, Nagy A, Chowdhury S, Crocker N, Degrandchamp G, McLean A, Gage K, Marinoni A, Martin E, Ronchi G and the DIII-D Team 2024 *Nucl. Fusion* **64** 126058
[14] Ono M 1995 *Physics of Plasmas* **2** 4075
[15] Chiu S, Chan V, Harvey R and Porkolab M 1989 *Nucl. Fusion* **29** 2175
[16] Stix T H 1992 *Waves in plasmas* (Springer Science & Business Media)
[17] Harvey R and McCoy M 1992 The CQL3D fokker-planck code *Proceedings of the IAEA Technical Committee Meeting on Simulation and Modeling of Thermonuclear Plasmas* pp. 489–526
[18] Monticello D 1993 *Nucl. Fusion* **33** 359
[19] Lu L, Lu B, Zhang X, Colas L, Urbanczyk G, Wang Z, Li Z, Hao B, Xue L, Xue M, Wang S and Sun A 2023 *Nucl. Fusion* **63** 066023
[20] Xue M, Zheng G Y, Xue L, Li J X, Wang S, Du H L, Zhu Y R and Zhou Y 2024 *Chin. Phys. B* **33** 084703
[21] Lin W H, Li J Q, Garcia J and Mazzi S 2023 *Chin. Phys. B* **32** 025202
[22] Bertelli N, Valeo E J, Green D L, Gorelenkova M, Phillips C K, Podestà M, Lee J P, Wright J C and Jaeger E F 2017 *Nucl. Fusion* **57** 056035
[23] Li X X, Liu H B, Xiang N and Li M H 2020 *Phys. Lett. A* **384** 126779
[24] Xue L, Garcia J, Zheng G, Hoang G, Artaud J, Duan X, Li J, Giruzzi G, Zou X, Pan W, Zhang J, Huang M, Wei H, Bai X, Ji X, Song X, Wang S, Song X, Xue M, Huang W and the HL-2M team 2019 *Nucl. Fusion* **60** 016016
[25] Liu H B, Li X X, Xiao Z Y, Zhang D Z and Sun A P 2021 *Journal of the Korean Physical Society* **79** 1135